Well-balanced methods for the Shallow Water equations in spherical coordinates.

Manuel J. Castro, Sergio Ortega, Carlos Parés
University of Málaga (Spain)

August 30, 2017

Dedicated to Tito Toro, maestro y amigo, on the occasion of his 70th anniversary

Abstract

The goal of this work is to obtain a family of explicit high order well-balanced methods for the shallow water equations in spherical coordinates. Application of shallow water models to large scale problems requires the use of spherical coordinates: this is the case, for instance, of the simulation of the propagation of a Tsunami wave through the ocean. Although the PDE system is similar to the shallow water equations in Cartesian coordinates, new source terms appear. As a consequence, the derivation of high order numerical methods that preserve water at rest solutions is not as straightforward as in that case. Finite Volume methods are considered based on a first order path-conservative scheme and high order reconstruction operators. Numerical methods based on these ingredients have been successfully applied previously to the nonlinear SWEs in Cartesian coordinates. Some numerical tests to check the well-balancing and high order properties of the scheme, as well as its ability to simulate planetary waves or tsunami waves over realistic bathymetries are presented.

Keywords: Shallow water model, well-balanced methods, finite volume methods, approximate Riemann solvers, high order methods.
Acknowledgments. The authors would like to thank the anonymous reviewers of the article for their valuable comments and suggestions. This research has been partially supported by the Spanish Government and FEDER through Research project MTM2015-70490-C2-1-R and Andalusian Government Research projects P11-FQM-8179 and P11-RNM-7069.

1 Introduction

The shallow water equations (SWEs) are useful to model free surface gravity waves whose wavelength is much larger than the characteristic bottom depth: see [39, 40, 41] for a review of these equations. This is the case of tsunami waves: although the depth bottom of the oceans cannot be considered as small, the characteristic wavelength of a tsunami can be of the order of 100km, what is significantly larger than the characteristic ocean depth.

On the other hand, the application of SWE to large scale phenomena (of the order of 1000's of km) makes necessary to take into account the curvature of the Earth. Usually, the Earth is approached by a sphere and the equations are written in spherical coordinates. Although the PDE system is similar to the SWEs in the plane using Cartesian coordinates, new source terms appear

due to the change of variables. Therefore, the discretization of the system in spherical coordinates goes far beyond a simple adaptation of the numerical methods for the equations written in Cartesian coordinates.

SWEs in spherical coordinates are the basis of many of the most used software packages for tsunami simulations. In most cases, the linear SWEs are considered, what is enough to give an acceptable simulation of the propagation of the wave in deep waters: [32, 2]. Nevertheless, the linear SWEs cannot be used for the simulation of the arrival of the wave to the shore and the subsequent flooding. On the other hand, when the nonlinear SWEs are considered, in most cases the formulation in primitive variables (i.e. velocity/thickness) is used instead of the conserved ones (discharge/thickness): see [31]. While the systems written in one or another set of variables is equivalent for smooth solutions, this is not the case when shock waves develop: the jump condition depends on the formulation, and the one consistent with the physics of the system is the one corresponding to the formulation in conserved variables. Again, while the formation of shock waves is not expected during the propagation of the wave, it is very likely to happen when the wave is close to the shore.

Finally, in some cases the nonlinear SWEs in spherical coordinates using the conserved variables is used, but some of the source terms due to the change of variables are neglected, as their influence is not relevant far enough of the poles (see [32]).

In this article, we consider the nonlinear SWEs in conserved variables formulation with all the source terms related to bottom variations and to the curvature. Neither Coriolis force (whose influence is not relevant for Tsunami waves) nor friction forces (whose numerical treatment can be done like in the Cartesian coordinates case) are considered.

Our goal is to derive an explicit high order well-balanced numerical scheme. By well-balanced, we mean that stationary solutions corresponding to water at rest situations have to be preserved by the numerical methods, what is a standard requirement in the context of SWEs: [3], [1], [4], [12], [22], [23], [26], [27], [33], [35], [42], [30], among others. Finite Volume methods considered here are based on a first order path-conservative scheme for the standard 1d SWEs and on high order reconstruction operators. Numerical methods based on these ingredients have been successfully applied previously to the nonlinear SWEs in Cartesian coordinates: [7], [6], [15], [27], [18], [17]. A recent review on these methods can be found in [8].

The organization of the article is as follows: in next section, the PDE system is introduced and an equivalent formulation is obtained which is better suited to the application of Finite Volume methods. In Section 3 the general form of the semidiscrete in space numerical method is introduced. Next, a general result concerning the well-balanced property of the method is proved: if the first order path-conservative scheme and the reconstruction operator are both well-balanced (in a sense to be specified) then the high order numerical method is well-balanced as well. A general way of obtaining well-balanced first order schemes and well-balanced high order reconstruction operators based respectively on [11] and [9] is also introduced. We also discuss the influence of the quadrature formulas used to approximate the volume and line integrals of the scheme in the well-balancing property. Some numerical tests are introduced in Section 5 in order to check the well-balancing and high order properties of the method, as well as its ability to simulate planetary waves or tsunami waves over a realistic bathymetry of the Mediterranean Sea. Finally, some conclusions are drawn.

2 PDE System

The shallow water equations on the sphere writes in spherical coordinates as follows (see [40] and references therein)

$$\begin{cases} \partial_t h + \dfrac{1}{R\cos(\varphi)}\Big(\partial_\theta(hu_\theta) + \partial_\varphi(hu_\varphi\cos(\varphi))\Big) = 0, \\ \partial_t u_\theta + \dfrac{u_\theta}{R\cos(\varphi)}\partial_\theta u_\theta + \dfrac{u_\varphi}{R}\partial_\varphi u_\theta - \dfrac{u_\theta u_\varphi}{R}\tan(\varphi) + \dfrac{g}{R\cos(\varphi)}\partial_\theta h = \dfrac{g}{R\cos(\varphi)}\partial_\theta H, \\ \partial_t u_\varphi + \dfrac{u_\theta}{R\cos(\varphi)}\partial_\theta u_\varphi + \dfrac{u_\varphi}{R}\partial_\varphi u_\varphi + \dfrac{u_\theta^2}{R}\tan(\varphi) + \dfrac{g}{R}\partial_\varphi h = \dfrac{g}{R}\partial_\varphi H, \end{cases} \tag{1}$$

where R is the radius; (θ, φ), the longitude and latitude; g, the gravity; h, the thickness of the water layer; H, the bottom depth; u_θ, u_φ, are the longitudinal and latitudinal velocities averaged in the normal direction.

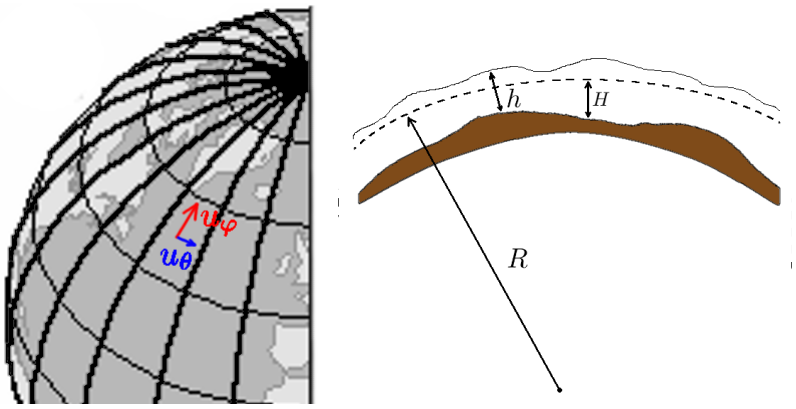

Figure 1: Sketch of the unknowns for the shallow-water equations in spherical coordinates.

As it is well known, when shock waves develop, the Rankine-Hugoniot conditions depend on the formulation of the system. Moreover, the Rankine-Hugoniot conditions related to the system written in velocity-thickness formulation are not the physically correct jump conditions. Therefore, we will consider the discharge-thickness formulation:

$$\begin{cases} \partial_t h + \dfrac{1}{R\cos(\varphi)}\Big(\partial_\theta q_\theta + \partial_\varphi(q_\varphi\cos(\varphi))\Big) = 0, \\ \partial_t q_\theta + \dfrac{1}{R\cos(\varphi)}\partial_\theta\left(\dfrac{q_\theta^2}{h}\right) + \dfrac{1}{R}\partial_\varphi\left(\dfrac{q_\theta q_\varphi}{h}\right) - 2\dfrac{q_\theta q_\varphi}{Rh}\tan(\varphi) + \dfrac{gh}{R\cos(\varphi)}\partial_\theta h = \dfrac{gh}{R\cos(\varphi)}\partial_\theta H, \\ \partial_t q_\varphi + \dfrac{1}{R\cos(\varphi)}\partial_\theta\left(\dfrac{q_\varphi q_\theta}{h}\right) + \dfrac{1}{R}\partial_\varphi\left(\dfrac{q_\varphi^2}{h}\right) + \dfrac{(q_\theta^2 - q_\varphi^2)}{hR}\tan(\varphi) + \dfrac{gh}{R}\partial_\varphi h = \dfrac{gh}{R}\partial_\varphi H, \end{cases} \tag{2}$$

where

$$q_\theta = hu_\theta, \quad q_\varphi = hu_\varphi.$$

In order to write the equations in the form of a system of balance laws, the following variables are introduced

$$h_\sigma = h\cos(\varphi), \quad H_\sigma = H\cos(\varphi), \quad \eta_\sigma = h_\sigma - H_\sigma, \quad Q_\varphi = \cos(\varphi)q_\varphi, \quad Q_\theta = \cos(\varphi)q_\theta,$$

and the system is rewritten as follows:

$$\begin{cases} \partial_t h_\sigma + \dfrac{1}{R}\Big(\partial_\theta\left(\dfrac{Q_\theta}{\cos(\varphi)}\right) + \partial_\varphi Q_\varphi\Big) = 0, \\ \partial_t Q_\theta + \dfrac{1}{R}\partial_\theta\left(\dfrac{Q_\theta^2}{h_\sigma\cos(\varphi)}\right) + \dfrac{1}{R}\partial_\varphi\left(\dfrac{Q_\theta Q_\varphi}{h_\sigma}\right) - \dfrac{Q_\theta Q_\varphi}{Rh_\sigma}\tan(\varphi) + \dfrac{gh_\sigma}{R\cos^2(\varphi)}\partial_\theta\eta_\sigma = 0, \\ \partial_t Q_\varphi + \dfrac{1}{R}\partial_\theta\left(\dfrac{Q_\varphi Q_\theta}{h_\sigma\cos(\varphi)}\right) + \dfrac{1}{R}\partial_\varphi\left(\dfrac{Q_\varphi^2}{h_\sigma}\right) + \left(\dfrac{Q_\theta^2}{Rh_\sigma} + \dfrac{gh_\sigma\eta_\sigma}{R\cos(\varphi)}\right)\tan(\varphi) + \dfrac{gh_\sigma}{R\cos(\varphi)}\partial_\varphi\eta_\sigma = 0. \end{cases} \tag{3}$$

Remark 1. *Since* $\cos(\varphi)$ *is continuous, it can be easily checked that the Rankine-Hugoniot conditions corresponding to systems* (2) *and* (3) *are equivalents. Moreover, if* H *is assumed to be smooth, then the products* $h_\sigma\partial_\theta\eta_\sigma$ *and* $h_\sigma\partial_\varphi\eta_\sigma$ *are well defined.*

Remark 2. *Let* O *be a domain in the* θ-φ *plane such that* q_θ *and* q_φ *vanish on its boundary. Then, the first equation implies that*

$$R\int_O h_\sigma\, d\mathbf{x} = \int_O hR\cos(\varphi)\, d\theta d\varphi = \int_{\mathcal{O}} h\, d\gamma$$

is preserved, where $\mathcal{O}$ *is the image of* O *on the sphere of radius* R*. Notice that this quantity is different from the water mass, whose expression (assuming that the water density is 1) is given by:*

$$\int_{\mathcal{O}} h d\gamma + \int_{\mathcal{O}}\left(\frac{h}{R}\frac{\eta - H}{2}\right) d\gamma.$$

Nevertheless the difference is small if $h \ll R$*, what it is usually the case.*

Finally, we introduce the variable $\sigma = \cos(\varphi)$ that allows us to write the system as follows:

$$\begin{cases} \partial_t h_\sigma + \dfrac{1}{R}\Big(\partial_\theta\left(\dfrac{Q_\theta}{\sigma}\right) + \partial_\varphi Q_\varphi\Big) = 0, \\ \partial_t Q_\theta + \dfrac{1}{R}\partial_\theta\left(\dfrac{Q_\theta^2}{h_\sigma\sigma}\right) + \dfrac{1}{R}\partial_\varphi\left(\dfrac{Q_\theta Q_\varphi}{h_\sigma}\right) + \dfrac{Q_\theta Q_\varphi}{Rh_\sigma\sigma}\partial_\varphi\sigma + \dfrac{gh_\sigma}{R\sigma^2}\partial_\theta\eta_\sigma = 0, \\ \partial_t Q_\varphi + \dfrac{1}{R}\partial_\theta\left(\dfrac{Q_\varphi Q_\theta}{h_\sigma\sigma}\right) + \dfrac{1}{R}\partial_\varphi\left(\dfrac{Q_\varphi^2}{h_\sigma}\right) - \left(\dfrac{Q_\theta^2}{Rh_\sigma\sigma} + \dfrac{gh_\sigma\eta_\sigma}{R\sigma^2}\right)\partial_\varphi\sigma + \dfrac{gh_\sigma}{R\sigma}\partial_\varphi\eta_\sigma = 0, \\ \partial_t\sigma = 0. \end{cases} \tag{4}$$

The system can be written in the more compact form:

$$\partial_t W + \frac{1}{R}\Big(\partial_\theta\tilde{F}_\theta(W) + \partial_\varphi\tilde{F}_\varphi(W) + \tilde{T}_\theta^p(W)\partial_\theta\eta_\sigma + \tilde{T}_\varphi^p(W)\partial_\varphi\eta_\sigma + \tilde{G}_\varphi(W)\partial_\varphi\sigma\Big) = 0, \tag{5}$$

where

$$W = \begin{bmatrix} w \\ \sigma \end{bmatrix} = \begin{bmatrix} h_\sigma \\ Q_\theta \\ Q_\varphi \\ \sigma \end{bmatrix} \tag{6}$$

$$\tilde{F}_\theta(W) = \begin{bmatrix} F_\theta(W) \\ 0 \end{bmatrix} = \begin{bmatrix} \dfrac{Q_\theta}{\sigma} \\ \dfrac{Q_\theta^2}{h_\sigma \sigma} \\ \dfrac{Q_\varphi Q_\theta}{h_\sigma \sigma} \\ 0 \end{bmatrix}, \quad \tilde{F}_\varphi(W) = \begin{bmatrix} F_\varphi(w) \\ 0 \end{bmatrix} = \begin{bmatrix} Q_\varphi \\ \dfrac{Q_\theta Q_\varphi}{h_\sigma} \\ \dfrac{Q_\varphi^2}{h_\sigma} \\ 0 \end{bmatrix} \tag{7}$$

$$\tilde{T}_\theta^p(W) = \begin{bmatrix} T_\theta^p(W) \\ 0 \end{bmatrix} = \begin{bmatrix} 0 \\ \dfrac{g h_\sigma}{\sigma^2} \\ 0 \\ 0 \end{bmatrix}, \quad \tilde{T}_\varphi^p(W) = \begin{bmatrix} T_\varphi^p(W) \\ 0 \end{bmatrix} = \begin{bmatrix} 0 \\ 0 \\ \dfrac{g h_\sigma}{\sigma} \\ 0 \end{bmatrix}, \tag{8}$$

$$\tilde{G}_\varphi(W) = \begin{bmatrix} G_\varphi(W) \\ 0 \end{bmatrix}; \quad G_\varphi(W) = G_\varphi^1(W) + G_\varphi^2(h_\sigma, \eta_\sigma, \sigma); \tag{9}$$

$$G_\varphi^1(W) = \begin{bmatrix} 0 \\ \dfrac{Q_\theta Q_\varphi}{h_\sigma \sigma} \\ -\dfrac{Q_\theta^2}{h_\sigma \sigma} \end{bmatrix}; \quad G_\varphi^2(h_\sigma, \eta_\sigma, \sigma) = \begin{bmatrix} 0 \\ 0 \\ -\dfrac{g h_\sigma \eta_\sigma}{\sigma^2} \end{bmatrix}. \tag{10}$$

In practice, the trivial equation for σ will be dropped and the system will be written as follows:

$$\partial_t w + \frac{1}{R}\left(\partial_\theta F_\theta(W) + \partial_\varphi F_\varphi(W) + T_\theta^p(W)\partial_\theta \eta_\sigma + T_\varphi^p(W)\partial_\varphi \eta_\sigma + G_\varphi(W)\partial_\varphi \sigma\right) = 0. \tag{11}$$

The advective flux $\vec{F} = (F_\theta, F_\varphi)$ and the pressure term $\vec{T}^p = (T_\theta^p, T_\varphi^p)$ satisfy the following rotational invariance-like properties: given a state W and a unit vector $\vec{n} = [n_\theta, n_\varphi]^T$ one has

$$R_{\vec{\nu}} F_{\vec{n}}(W) = \delta\, F(R_{\vec{\nu}} w), \quad R_{\vec{\nu}} T_{\vec{n}}^p(W) = \delta\, T^p\left(\frac{h_\sigma}{\sigma}\right), \tag{12}$$

where

$$F_{\vec{n}}(W) = n_\theta F_\theta(W) + n_\varphi F_\varphi(W), \quad T_{\vec{n}}^p(W) = n_\theta T_\theta^p(W) + n_\varphi T_\varphi^p(W), \tag{13}$$

$$\delta = \sqrt{\frac{n_\theta^2}{\sigma^2} + n_\varphi^2}, \quad \vec{\nu} = \begin{bmatrix} \nu_\theta \\ \nu_\varphi \end{bmatrix} = \begin{bmatrix} \dfrac{n_\theta}{\sigma\delta} \\ \dfrac{n_\varphi}{\delta} \end{bmatrix}, \quad \vec{\nu}^\perp = \begin{bmatrix} -\nu_\varphi \\ \nu_\theta \end{bmatrix}, \tag{14}$$

$$R_{\vec{\nu}} = \begin{bmatrix} 1 & 0 & 0 \\ 0 & \nu_\theta & \nu_\varphi \\ 0 & -\nu_\varphi & \nu_\theta \end{bmatrix}. \tag{15}$$

and, for every $U_\sigma = [h_\sigma, Q_{\vec{\nu}}, Q_{\vec{\nu}^\perp}]^T$ and h:

$$F(U_\sigma) = \begin{bmatrix} Q_{\vec{\nu}} \\ \dfrac{Q_{\vec{\nu}}^2}{h_\sigma} \\ \dfrac{Q_{\vec{\nu}} Q_{\vec{\nu}^\perp}}{h_\sigma} \end{bmatrix}, \quad T^p(h) = \begin{bmatrix} 0 \\ gh \\ 0 \end{bmatrix}. \tag{16}$$

3 Numerical methods

Let us first describe the general form of a semidiscrete in space high order method for (11). Given a domain Ω in the θ-φ plane, we consider a partition in cells $\mathcal{T} = \{V_i\}_{i=1}^{NC}$ with the usual properties: the cells are closed convex polygons and the intersection of two cells can only be a vertex, an edge, or empty. Two cells V_i and V_j are said to be neighbors it they share an edge $E_{i,j}$. $\vec{n}_{i,j} = [n_{i,j}^{\theta}, n_{i,j}^{\varphi}]^T$ represents the unit vector normal to $E_{i,j}$ pointing from V_i to V_j, therefore:

$$\vec{n}_{i,j} = -\vec{n}_{j,i}.$$

$|V_i|$ and $|E_{i,j}|$ represent the area of V_i and the length of $E_{i,j}$ respectively. Given a cell V_i, we denote by $\mathcal{N}_i$ the set of indexes of the neighbors of V_i. Finally, $\Delta\mathbf{x}$ represents the maximum of the diameters of the cells.

The approximation of the average of the solution at the cell V_i at time t will be represented by:

$$w_i(t) = \begin{bmatrix} h_{\sigma,i}(t) \\ Q_{\theta,i}(t) \\ Q_{\varphi,i}(t) \end{bmatrix}.$$

The following notation will be also used:

$$W_i(t) = \begin{bmatrix} w_i(t) \\ \bar{\sigma}_i \end{bmatrix},$$

where $\bar{\sigma}_i$ is the exact average of σ at the cell: remember that $\sigma = \cos(\varphi)$ is known.

Let us consider a high order reconstruction operator that, given a set of cell averages $\{w_i\}_{i=1}^{NC}$, provides for every cell V_i a smooth function

$$p_i(\mathbf{x}) = p_i(\mathbf{x}; \{w_j\}_{j \in S_i}), \quad \mathbf{x} = (\theta, \varphi),$$

computed by interpolation or approximation from the averages at the cells whose indexes belong to the set S_i called the stencil of V_i. The following notation will be used:

$$w_{i,j}^{-}(\gamma) = \lim_{\mathbf{x} \in V_i \to \gamma} p_i(\mathbf{x}), \quad w_{i,j}^{+}(\gamma) = \lim_{\mathbf{x} \in V_j \to \gamma} p_j(\mathbf{x}), \quad \forall \gamma \in E_{i,j}.$$

The following equalities hold:

$$w_{i,j}^{-}(\gamma) = w_{j,i}^{+}(\gamma), \quad w_{i,j}^{+}(\gamma) = w_{j,i}^{-}(\gamma).$$

The reconstruction operator is assumed to be conservative, i.e.

$$w_i = \frac{1}{|V_i|} \int_{V_i} p_i(\mathbf{x})\, d\mathbf{x}, \quad \forall i,$$

and high order accurate in the following sense: there exists a natural s such that, if the operator is applied at the cell averages $\{\bar{w}_i\}_{i=1}^{NC}$ of a smooth function $w : \Omega \to \mathbb{R}$, then:

$$w_{i,j}^{\pm}(\gamma) = w(\gamma) + O(\Delta\mathbf{x}^s), \quad w_{i,j}^{+} - w_{i,j}^{-} = O(\Delta\mathbf{x}^{s+1}), \quad \forall \gamma \in E_{i,j},$$

$$p_i(\mathbf{x}) = w(\mathbf{x}) + O(\Delta\mathbf{x}^s), \quad \forall \mathbf{x} \in \mathring{V}_i.$$

Some examples of high order reconstruction operators satisfying the previous properties have been introduced in [20], [34], [16], [25], [17], [13], etc.

The expression of the semidiscrete method is then as follows:

$$
\begin{aligned}
w_i'(t) \;=\; & -\frac{1}{R|V_i|}\left(\sum_{j\in\mathcal{N}_i}\left(\int_{E_{i,j}} F_{\vec{n}_{i,j}}(W_{i,j}^-(\gamma))\,d\gamma + \int_{E_{i,j}} \delta_{i,j}(\gamma) D_{i,j}^-(\gamma)\,d\gamma\right)\right. \\
& + \int_{V_i}\left(T_\theta^p(P_i(\mathbf{x}))\partial_\theta p_{\eta_\sigma,i}(\mathbf{x}) + T_\varphi^p(P_i(\mathbf{x}))\partial_\varphi p_{\eta_\sigma,i}(\mathbf{x})\right)\,d\mathbf{x} \\
& \left. + \int_{V_i} G_\varphi(P_i(\mathbf{x}))\partial_\varphi\sigma(\mathbf{x})\,d\mathbf{x}\right).
\end{aligned}
\tag{17}
$$

The first integral on the right-hand side comes from the application of the divergence theorem to the advective flux term; the second one takes into account the jumps of the flux and the source terms across the edges; the third and fourth ones are the integrals in V_i of the source terms. The following notation has been used:

$$
P_i(\mathbf{x}) = \begin{bmatrix} p_{h_\sigma,i}(\mathbf{x}) \\ p_{Q_\theta,i}(\mathbf{x}) \\ p_{Q_\varphi,i}(\mathbf{x}) \\ \sigma(\mathbf{x}) \end{bmatrix}, \quad W_{i,j}^\pm(\gamma) = \begin{bmatrix} w_{i,j}^\pm(\gamma) \\ \sigma(\gamma) \end{bmatrix} = \begin{bmatrix} h_{\sigma,i,j}^\pm(\gamma) \\ Q_{\theta,i,j}^\pm(\gamma) \\ Q_{\varphi,i,j}^\pm(\gamma) \\ \sigma(\gamma) \end{bmatrix},
\tag{18}
$$

represent the reconstructions of $\{h_{\sigma,i}\}$, $\{Q_{\theta,i}\}$, $\{Q_{\varphi,i}\}$ at $\mathbf{x}\in\mathring{V}_i$ and at $\gamma\in E_{i,j}$ respectively; $p_{\eta_\sigma,i}(\mathbf{x})$ and $\eta_{\sigma,i,j}^\pm(\gamma)$ represent the reconstruction of $\{\eta_{\sigma,i}\}$ at $\mathbf{x}\in\mathring{V}_i$ and at $\gamma\in E_{i,j}$ respectively;

$$
\delta_{i,j}(\gamma) = \sqrt{\left(\frac{n_{i,j}^\theta}{\sigma(\gamma)}\right)^2 + (n_{i,j}^\varphi)^2}, \quad \vec{\nu}_{i,j}(\gamma) = \begin{bmatrix} \dfrac{n_{i,j}^\theta}{\sigma(\gamma)\delta_{i,j}(\gamma)} \\ \dfrac{n_{i,j}^\varphi}{\delta_{i,j}(\gamma)} \end{bmatrix}.
\tag{19}
$$

Finally,

$$
D_{i,j}^-(\gamma) = R_{\vec{\nu}_{i,j}(\gamma)}^{-1}\cdot D^-(R_{\vec{\nu}_{i,j}(\gamma)} w_{i,j}^-(\gamma), \eta_{\sigma,i,j}^-; R_{\vec{\nu}_{i,j}(\gamma)} w_{i,j}^+(\gamma), \eta_{\sigma,i,j}^+).
\tag{20}
$$

Here, $D^-(w_{\sigma,l},\eta_{\sigma,l};w_{\sigma,r},\eta_{\sigma,r})$ is the fluctuation function of a first-order path-conservative method (see [29, 8]) for the 1d system of balance laws:

$$
\partial_t U_\sigma + \partial_x F(U_\sigma) + T^p(h)\partial_x\eta_\sigma = 0,
\tag{21}
$$

where the rotational invariance-like properties have been used. Notice that (21) is nothing but the 1d shallow water system, with gravity constant g/σ and a transport equation for the tangential velocity $\frac{Q_{\vec{p}^\perp}}{h_\sigma}$.

Remark 3. *The source term $G_\varphi(W)\partial_\varphi\sigma$ does not contribute to the line integrals in* (17) *since $\sigma(\mathbf{x}) = \cos(\varphi)$ is continuous.*

Remark 4. *Instead of reconstructing H or H_σ, we choose to reconstruct η_σ: the reasons will be clear in next section.*

The discretization in time is then performed by applying to the ODE system (17) a high order numerical method: TVD RK method will be considered here (see [19]).

4 Well balancing

The stationary solutions corresponding to water at rest are given by

$$u_\varphi = 0, \quad u_\theta = 0, \quad \eta_\sigma = \bar{\eta}\cos(\varphi), \tag{22}$$

where $\bar{\eta}$ is a constant associated to the elevation of the undisturbed water. Following [29, 8], let us state the following definitions:

Definition 1. *The fluctuation function $D^-(U_{\sigma,l}, \eta_{\sigma,l}; U_{\sigma,r}, \eta_{\sigma,r})$ of a path-conservative method for solving* (21) *is said to be well-balanced if*

$$D^-\left(\begin{bmatrix} h_\sigma \\ 0 \\ 0 \end{bmatrix}, \eta_\sigma; \begin{bmatrix} h_{\sigma,r} \\ 0 \\ 0 \end{bmatrix}, \eta_\sigma\right) = 0, \forall\ h_{\sigma,l}, h_{\sigma,r}, \eta_\sigma. \tag{23}$$

Definition 2. *The reconstruction operator is said to be well-balanced if, given a water at rest solution w satisfying* (22)*, the reconstruction of its cell averages satisfy*

$$p_{Q_\theta,i}(\mathbf{x}) = 0, \quad p_{Q_\varphi,i}(\mathbf{x}) = 0, \quad p_{\eta_\sigma,i}(\mathbf{x}) = \bar{\eta}\cos(\varphi), \quad \forall \mathbf{x} \in V_i \tag{24}$$

for every i.

The following result holds:

Theorem 1. *If the fluctuation function D^- and the reconstruction operator are well-balanced, then* (17) *is well-balanced, i.e. water at rest solutions are preserved.*

Proof. Let us apply the numerical method (17) to the cell averages of a water at rest solution satisfying (22). From (24) we deduce

$$G_\varphi(P_i(\mathbf{x}))\partial_\varphi\sigma(\mathbf{x}) = G^2_\varphi(p_{h_\sigma,i}, p_{\eta_\sigma,i}, \sigma)\partial_\varphi\sigma(\mathbf{x}) = \begin{bmatrix} 0 \\ 0 \\ g p_{h_\sigma,i}\bar{\eta}\tan(\varphi) \end{bmatrix},$$

$$T^p_\theta(P_i(\mathbf{x}))\partial_\theta P_{\eta_\sigma,i}(\mathbf{x}) + T^p_\varphi(P_i(\mathbf{x}))\partial_\varphi P_{\eta_\sigma,i}(\mathbf{x}) = \begin{bmatrix} 0 \\ 0 \\ -g p_{h_\sigma,i}\bar{\eta}\tan(\varphi) \end{bmatrix},$$

and thus the cell integrals in (17) vanish. Finally, since the reconstruction operator is assumed to be exact for the null function, then

$$F_{\vec{n}_{i,j}}(W^-_{i,j}(\gamma)) = 0, \quad \forall \gamma \in E_{i,j};$$

and, since

$$R_{\vec{\nu}_{i,j}(\gamma)} w^\pm_{i,j}(\gamma) = [h^\pm_{\sigma,i,j}, 0, 0]^T,$$

and

$$\eta^\pm_{\sigma,i,j}(\gamma) = \bar{\eta}\cos(\gamma).$$

then (23) implies

$$D_{i,j}(\gamma) = R^{-1}_{\vec{\nu}_{i,j}(\gamma)} \cdot D(R_{\vec{\nu}_{i,j}(\gamma)} w^-_{i,j}(\gamma), \eta^-_{\sigma,i,j}; R_{\vec{\nu}_{i,j}(\gamma)} w^+_{i,j}(\gamma), \eta^+_{\sigma,i,j}) = 0, \quad \forall \gamma \in E_{i,j}.$$

Therefore the line integrals also vanish. Summing up, the cell averages of a stationary solution corresponding to water at rest constitute an equilibrium of the ODE system (17).

□

4.1 Well-balanced fluctuations

Concerning the well-balanced fluctuation, following [11], we consider the one corresponding to a PVM method:

$$D^-(U_{\sigma,l},\eta_{\sigma,l};U_{\sigma,r},\eta_{\sigma,r}) = \frac{1}{2}\left(I - Q_{1/2}J_{1/2}^{-1}\right)\left(F(U_{\sigma,r}) - F(U_{\sigma,l}) + T^p(h_{1/2})(\eta_{\sigma,r}-\eta_{\sigma,l})\right) \quad (25)$$

where I is the identity matrix;

$$h_{1/2} = \frac{h_l + h_r}{2};$$

$J_{1/2}$ is the standard Roe matrix for system (21); and $Q_{1/2}$ is a viscosity matrix that is computed by evaluating a given polynomial at $J_{1/2}$:

$$Q_{1/2} = P_l(J_{1/2}), \quad (26)$$

where

$$P_l(x) = \sum_{j=0}^{l} a_j^{1/2}\, x^j.$$

This method is path-conservative for the family of paths given by the straight segments (see [29]). Many numerical schemes may be considered as particular cases of PVM methods: this is the case for Roe method, HLL (see [21]), HLLC (see [38]) , FORCE (see [37]), WAF (see [36]), etc. The interested reader is referred to [11] and [10] for details. Observe that (23) is trivial: if $U_{\sigma,l} = [h_{\sigma,l}, 0, 0]$, $U_{\sigma,r} = [h_{\sigma,r}, 0, 0]$, $\eta_{\sigma,l} = \bar{\eta}\cos(\varphi_{1/2})$, and $\eta_{\sigma,l} = \bar{\eta}\cos(\varphi_{1/2})$ then

$$F(U_{\sigma,r}) - F(U_{\sigma,l}) + T^p(h_{1/2})(\eta_{\sigma,r}-\eta_{\sigma,l}) = 0.$$

Note that the numerical scheme is not well-defined if $J_{1/2}$ is not invertible. Here we follow [11] to redefine the fluctuation in this case.

4.2 Well-balanced reconstructions

In order to construct a well-balanced high order reconstruction operator, we follow the ansatz proposed in [9]. First, a standard high-oder accurate reconstruction operator

$$p_i(\mathbf{x}) = p_i(\mathbf{x}; \{w_j\}_{j\in S_i})$$

is considered such that

$$p_i(\mathbf{x}; \{0\}_{j\in S_i}) = 0, \quad \forall i,\ \forall \mathbf{x} \in V_i,$$

that is, the reconstruction operator is exact for the null function. The following stages are then pursued in the reconstruction procedure: given the cell averages $\{h_{\sigma,i}\}$, $\{Q_{\theta,i}\}$, $\{Q_{\varphi,i}\}$, $\{H_{\sigma,i}\}$, $\{\bar{\sigma}_i\}$

1. The reconstruction operator is applied to $\{h_{\sigma,i}\}$, $\{Q_{\theta,i}\}$, $\{Q_{\varphi,i}\}$, to obtain $p_{h_\sigma,i}$, $p_{Q_\theta,i}$, $p_{Q_\varphi,i}$ respectively.

2. The averages of η_σ at the cells are given by:

$$\eta_{\sigma,i} = h_{\sigma,i} - H_{\sigma,i}$$

and those of η are approached by:

$$\bar{\eta}_i = \frac{\eta_{\sigma,i}}{\bar{\sigma}_i}, \quad \forall i.$$

The fluctuations

$$f_j = \eta_{\sigma,j} - \bar{\eta}_i \bar{\sigma}_j, \quad j \in S_i$$

are computed. These fluctuations measure the distance between the cell averages in the stencil of the ith cell and those of the water at rest solution $u_\theta = 0$, $u_\varphi = 0$, $\eta_\sigma = \bar{\eta}_i \cos(\varphi)$.

3. The reconstruction operator is then applied to the fluctuations to obtain

$$p_{f,i}(\mathbf{x}) = p_{f,i}(\mathbf{x}; \{f_j\}_{j \in S_i}), \quad \forall i.$$

4. Finally, the reconstruction of η_σ is defined by:

$$p_{\eta_{\sigma,i}}(\mathbf{x}) = \bar{\eta}_i \cos(\varphi) + p_{f,i}(\mathbf{x}).$$

It can be easily shown that the accuracy of the modified reconstruction operator is equal to the one of the original operator and that (24) is satisfied, i.e. the reconstruction operator is well-balanced as $p_{f,i}(\mathbf{x}) = 0$ for any stationary solution (22). Moreover, the method can be equivalently written in terms of the reconstructed fluctuations as follows:

$$\begin{aligned} w_i'(t) \;=\; & -\frac{1}{R|V_i|}\left(\sum_{j \in \mathcal{N}_i} \left(\int_{E_{i,j}} F_{\vec{n}_{i,j}}(W_{i,j}^-(\gamma))\, d\gamma + \int_{E_{i,j}} \delta_{i,j}(\gamma) D_{i,j}^-(\gamma)\, d\gamma \right) \right. \\ & + \int_{V_i} \left(T_\theta^p(P_i(\mathbf{x})) \partial_\theta p_{f,i}(\mathbf{x}) + T_\varphi^p(P_i(\mathbf{x})) \partial_\varphi p_{f,i}(\mathbf{x}) \right) d\mathbf{x} \\ & \left. + \int_{V_i} \left(G_\varphi^1(P_i(\mathbf{x})) + G_\varphi^2(p_{h_\sigma}(\mathbf{x}), p_{f,i}(\mathbf{x}), \sigma(\mathbf{x})) \right) \partial_\varphi \sigma(\mathbf{x})\, d\mathbf{x} \right), \end{aligned} \tag{27}$$

where the equality

$$T_\theta^p(P_i(\mathbf{x})) \partial_\theta (\bar{\eta}_i \cos(\varphi)) + T_\varphi^p(P_i(\mathbf{x})) \partial_\varphi (\bar{\eta}_i \cos(\varphi)) + G_\varphi^2(p_{h_\sigma}, \bar{\eta}_i \cos(\varphi), \sigma) \partial_\varphi \cos(\varphi) = 0 \tag{28}$$

has been used.

Remark 5. *A well-balanced first order version of the method can be obtained as a particular case of the previous semi-discrete scheme by choosing the trivial reconstruction operator:*

$$p_i(\mathbf{x}) = p_i(\mathbf{x}; w_i) = w_i.$$

The reconstructions of all the variables are then piecewise constant but the one of η_σ that is defined as follows:

$$p_{\eta_{\sigma,i}}(\mathbf{x}) = \bar{\eta}_i \cos(\varphi) + \eta_{\sigma,i} - \bar{\eta}_i \cos(\varphi_i),$$

where $\mathbf{x}_i = (\theta_i, \varphi_i)$ represents the center of the volume V_i.

Note that, if we define $\bar{\sigma}_i = \cos(\varphi_i)$, then

$$p_{\eta_{\sigma,i}}(\mathbf{x}) = \frac{\eta_{\sigma,i}}{\cos(\varphi_i)} \cos(\varphi).$$

Finally, observe that, with this reconstruction, the numerical method is well-balanced in the sense that the point values at the center of the cells of a stationary solution corresponding to water at rest are preserved, what is the usual well-balanced requirement for first order methods.

4.3 Numerical integration

In practice, the integrals appearing in (17) are approached by using quadrature formulas whose order is bigger or equal to the one of the reconstruction operators:

$$\begin{aligned} w_i'(t) &= -\frac{1}{R|V_i|}\Big(\sum_{j\in\mathcal{N}_i}\left(|E_{i,j}|\sum_{l=0}^{k}\alpha_l F_{\vec{n}_{i,j}}(W_{i,j}^-(\gamma_{i,j}^l)) + |E_{i,j}|\sum_{l=0}^{k}\alpha_l\delta_{i,j}(\gamma_{i,j}^l)D_{i,j}^-(\gamma_{i,j}^l)\right)\\ &\quad+\sum_{l=0}^{K}\beta_l\left(T_\theta^p(P_i(\mathbf{x}_i^l))\partial_\theta p_{f,i}(\mathbf{x}_i^l) + T_\theta^p(P_i(\mathbf{x}_i^l))\partial_\varphi p_{f,i}(\mathbf{x}_i^l)\right)\\ &\quad+\sum_{l=0}^{K}\beta_l\left(G_\varphi^1(P_i(\mathbf{x}_i^l)) + G_\varphi^2(p_{h_\sigma}(\mathbf{x}_i^l), p_{f,i}(\mathbf{x}_i^l), \sigma(\mathbf{x}_i^l))\right)\partial_\varphi\sigma(\mathbf{x}_i^l)\Big), \end{aligned} \tag{29}$$

where $\{\gamma_{i,j}^l\}_{l=0}^k$, $\{\alpha_l\}_{l=0}^k$ are the quadrature points and weights of the formula chosen in $E_{i,j}$, and $\{\mathbf{x}_i^l\}_{l=0}^K$, $\{\beta_l\}_{l=0}^K$ those of the formula chosen in V_i.

The well-balanced property is preserved: notice that, in the proof of Theorem 1, it has been shown that the integrands vanish at every point, so that the approximations of the integrals by quadrature formulas also vanish.

The volume quadrature formula may be also used to compute the cell averages of the variable

$$\bar{w}_i = \sum_{l=0}^{K}\beta_l w(\mathbf{x}_l).$$

In that case, the modified reconstruction operator is still well-balanced provided that the averages of $\cos(\varphi)$ are computed by using the same quadrature formula, as it can be easily checked.

Remark 6. *In the particular case of a first order method mentioned in Remark 5, if the mid-point formulas are used, the expression of the numerical method is as follows:*

$$\begin{aligned} w_i'(t) &= -\frac{1}{R|V_i|}\Big(\sum_{j\in\mathcal{N}_i}\left(|E_{i,j}|F_{\vec{n}_{i,j}}(W_i) + |E_{i,j}|\delta_{i,j}(\gamma_{i,j})D_{i,j}^-(\gamma_{i,j})\right)\\ &\quad+\left(G_\varphi^1(W_i) - G_\varphi^2\left(h_i, \eta_{\sigma,i} - \bar{\eta}_i\cos(\varphi_i), \cos(\varphi_i)\right)\sin(\varphi_i)\right)\Big), \end{aligned}$$

where $\gamma_{i,j}$ is the midpoint of $E_{i,j}$.

5 Numerical tests

In this section we present some numerical tests in order to check the well-balancing and high order properties of the scheme, as well as its ability to simulate planetary waves or tsunami waves over realistic bathymetries. Here only structured grids on the θ-φ plane are considered. We use the HLLC scheme written as a PVM method following [14] and the third order reconstruction operator described in [17], that has a compact stencil. We use the three step TVD RK method [19] that is also third order accurate in time. The two-point Gauss quadrature formula is used for the line integrals and its natural extension to rectangular cells for the volume integrals. Therefore, the resulting scheme is third order accurate in space and time. The CFL condition reads as follows:

$$\Delta t = CFL\min_i\left\{\frac{R\Delta_\theta\Delta_\varphi\cos(\varphi_i)}{(|u_{\theta,i}| + \sqrt{gh_i})\Delta_\varphi + (|u_{\varphi,i}| + \sqrt{gh_i})\Delta_\theta}\right\}, \quad 0 \le CFL \le 1, \tag{30}$$

where Δ_θ and Δ_φ are the mesh sizes in the θ and φ directions.

In order to speedup the simulations, a parallel GPU implementation has been performed following the ideas described in [17] and [24].

Finally, we remark that although θ, φ are expressed in radians in the description of the numerical method, the description of the computational domains and initial data will be given in degrees, as it is customary in geophysics. Thus, the notation $\tilde{\theta}$ and $\tilde{\varphi}$ will be used to represent the longitude and latitude in degrees.

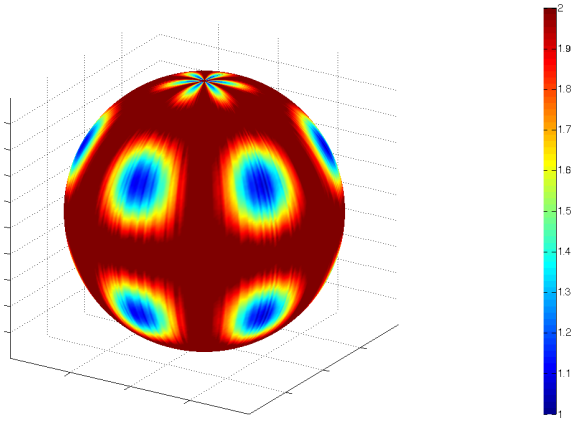

Figure 2: Well-balanced simulation: irregular bathymetry.

5.1 Water at rest simulation

The objective of this numerical test is to check the well-balanced property of the numerical scheme. We consider the rectangular domain $[-180, 180] \times [-89.5, 89.5]$ in the $\tilde{\theta}$-$\tilde{\varphi}$ plane (in degrees) that corresponds to a sphere with two polar caps. A uniform structured grid with $\Delta_{\tilde{\theta}} = \Delta_{\tilde{\varphi}} = 1^\circ$ is considered. The bathymetry is defined as follows: first we define the mean bathymetry

$$H_m(\tilde{\theta}, \tilde{\varphi}) = 2.0 - \cos^2\left(\frac{\pi\tilde{\theta}}{60}\right) \cdot \sin^2\left(\frac{\pi\tilde{\varphi}}{60}\right), \tag{31}$$

then $H(\tilde{\theta}, \tilde{\varphi})$ is defined by adding to H_m a uniform noise in the interval $[0, 0.2]$. Figure 2 shows the bathymetry for the realization presented here. Then, the initial water depth is set equal to the bathymetry, that is $h(\tilde{\theta}, \tilde{\varphi}, 0) = H(\tilde{\theta}, \tilde{\varphi})$ and $u_{\tilde{\varphi}} = u_{\tilde{\theta}} = 0$. The radius of the sphere is set to $R = 10000$ m. Periodic boundary conditions are prescribed in the eastern and western boundaries, and wall boundary conditions in the northern and southern boundaries corresponding to the polar caps. The CFL is set to 0.5 and a long time simulation is run. Table 1 present the evolution of the error in L^1-norm. As it can be seen, errors are of the order of the machine accuracy and the scheme is exactly well-balanced for the water at rest solution, as expected.

5.2 Propagation of a simple wave over an irregular geometry

In this test we simulate the evolution of a simple wave over an irregular geometry. Here we consider the same domain with a finer resolution: $\Delta_{\tilde{\theta}} = \Delta_{\tilde{\varphi}} = 0.25^\circ$ and the radius of the sphere is set

Time	Error
10m	$1.67E-15$
60m	$2.72E-15$
120m	$2.65E-15$

Table 1: Well-balanced solution: evolution of the error (L^1-norm).

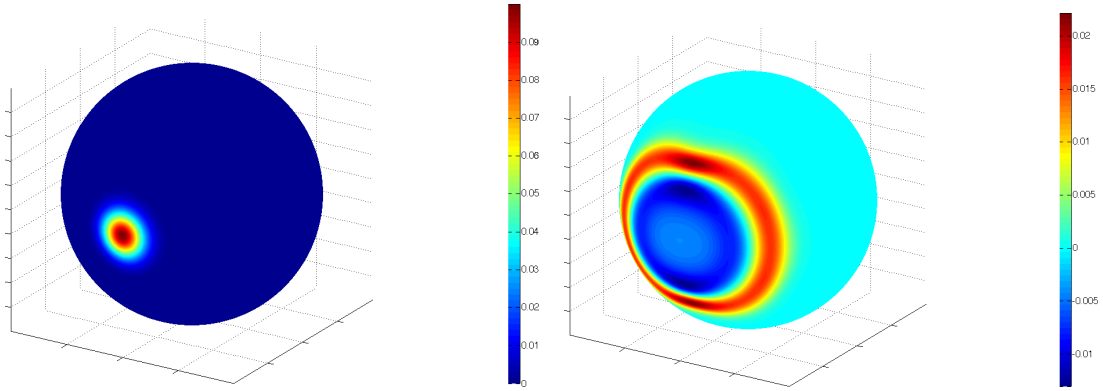

(a) Free surface at $t = 0$ minutes.

(b) Free surface at $t = 25$ minutes.

Figure 3: Evolution of the free surface over an irregular geometry.

to $R = 10000$ m. The CFL parameter is set to 0.5. The bathymetry $H(\tilde{\theta}, \tilde{\varphi})$ is given by the expression (31). The initial water thickness is given by

$$h(\tilde{\theta}, \tilde{\varphi}, 0) = H(\tilde{\theta}, \tilde{\varphi}) + 0.1e^{-\frac{\tilde{\theta}^2+\tilde{\varphi}^2}{100}},$$

and initial velocities are set to zero. Again, periodic boundary conditions are prescribed in the eastern and western boundaries, and wall boundary conditions in the northern and southern boundaries. Figures 3 and 4 show the evolution of the free surface. Note that no spurious oscillations appear during the wave propagation as the scheme is well-balanced. The wave starts moving from the equator towards the north and south poles (see Figures 3(b)-4(a)), collapses at the antipodes of the center of the initial solution, generates a wave moving opposite to the initial one, and finally comes back towards the initial location (see Figure 4(b)).

5.3 Numerical treatment of the poles

The use of spherical coordinate is not a priori well suited for the numerical simulation of waves on a complete sphere because of the singularities at the poles. If waves on a complete sphere are going to be simulated, the correct way to proceed in order to obtain high-order accurate solutions would be to consider at least an atlas of the sphere composed by two charts. Although the pole singularities are not a difficulty for geophysical water flows (which is our main field of application) due to the polar caps, we propose here a numerical treatment based on the use of two ghost cells. This treatment is not expected to be as accurate as the use of two different systems of local coordinates: the goal is to design a numerical treatment much less expensive and easy to implement giving acceptable simulations of waves passing through the poles.

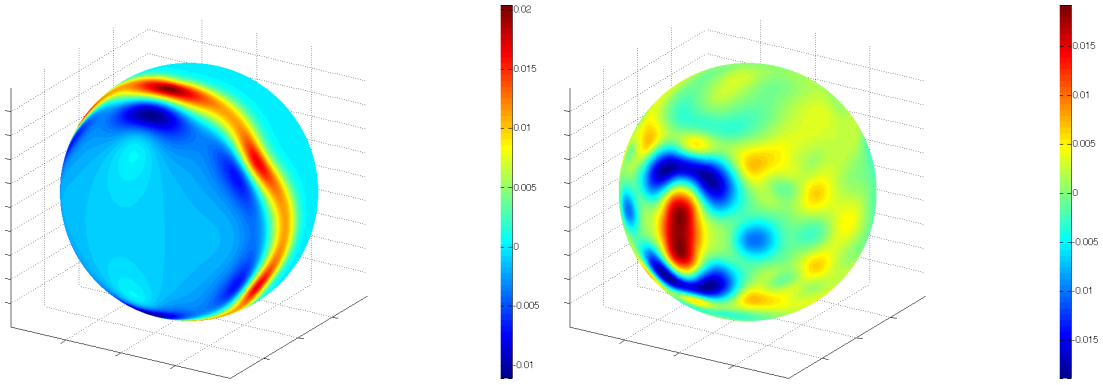

(a) Free surface at $t = 50$ minutes

(b) Free surface at $t = 240$ minutes

Figure 4: Evolution of the free surface over an irregular geometry.

The idea is as follows: for simplicity, let us consider a Cartesian grid of the domain $[-\pi, \pi] \times [-\pi/2, \pi/2]$ with steps

$$\Delta_\theta = \frac{2\pi}{N}, \quad \Delta_\varphi = \frac{\pi}{M}.$$

Let us define

$$\theta_i = -\pi + i\Delta_\theta, \quad 0 \le i \le N; \quad \varphi_j = -\frac{\pi}{2} + j\Delta_\varphi, \quad 0 \le j \le M.$$

Let us consider then the volumes

$$V_{i,j} = [\theta_{i-1}, \theta_i] \times [\varphi_{j-1}, \varphi_j], \quad 1 \le i \le N, 1 \le j \le M,$$

and denote by $\mathbf{x}_{i,j}$ their centers. $E_{i+1/2,j}$ represents the common edge to $V_{i,j}$ and $V_{i+1,j}$, and $E_{i,j+1/2}$ the common edge of $V_{i,j}$ and $V_{i,j+1}$. The computational domain is given by:

$$O = \bigcup_{\substack{1 \le i \le N \\ 2 \le j \le M-1}} V_{i,j}$$

and two ghost cells are considered

$$V_S = \bigcup_{1 \le i \le N} V_{i,1}, \quad V_N = \bigcup_{1 \le i \le N} V_{i,M}.$$

Observe that V_S and V_N are mapped onto two N-sided cells on the sphere that cover the poles. Moreover, the cells $V_{i,1}$ (resp. $V_{i,M}$), $1 \le i \le N$ map onto triangular subcells of the southern (resp. northern) ghost cell: see Figure 5. In particular, the edges $E_{i,1/2}$ (resp. $E_{i,M+1/2}$) map onto the south (resp. north) pole. Let us denote by $W_{i,j}(t) = [w_{i,j}(t), \bar{\sigma}_{i,j}]^T$ the numerical approximation at the computational cell $V_{i,j}$ at time t, and by $w_S(t)$, $w_N(t)$ the approximations at the ghost cells. Periodic boundary conditions are set in the eastern and western boundaries.

The following two-step strategies is proposed: once the values of the cell averages at time t_n, $W^n_{i,j}$, w^n_N, w^n_S, have been computed

1. the numerical method is applied to all the cells to obtain the next stage in the Runge-Kutta time stepping algorithm

$$w^{n+l}_{i,j}, \quad 1 \le i \le N, \quad 1 \le j \le M;$$

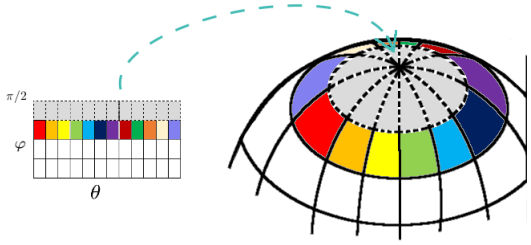

Figure 5: Sketch of the ghost cell in the north pole.

2. then

$$w_S^{n+l} = \frac{1}{N}\sum_{i=1}^{N} w_{i,1}^{n+l}, \quad w_N^{n+l} = \frac{1}{N}\sum_{i=1}^{N} w_{i,M}^{n+l}.$$

Remark 7. *In the first step of the algorithm:*

- *In the equations of $w_{i,N}$ (resp. $w_{i,1}$) there are no contributions from the edges $E_{i,M+1/2}$ (resp. $E_{i,1/2}$) since their lengths are 0 (remember that they map onto one of the poles). Moreover, the contributions from the edges $E_{i+1/2,1}$ or $E_{i+1/2,M}$ cancel since the values at the subcells of the ghost cells are identical.*
- *In the reconstruction step, lateral stencils are considered for the cells $V_{i,1}$, $V_{i,M}$.*
- *In order to avoid divisions by zero in the integral terms of the equations for $w_{i,1}$ or $w_{i,N}$, interior quadrature points have to be chosen.*

Remark 8. *For a first order numerical method, the resulting scheme is a standard finite volume method in which the values at the northern and southern cells are updated by computing the numerical fluxes between these cells and their neighbors.*

In order to test this strategy, we simulate the evolution of a small perturbation through the North pole. A Cartesian mesh of the rectangle $[-180, 180] \times [-90, 90]$ (in degrees) with $\Delta_{\tilde{\theta}} = \Delta_{\tilde{\varphi}} = 0.5°$ is considered. The depth is assumed to be constant $H(\tilde{\theta}, \tilde{\varphi}) = 1$m and the initial water thickness is given by

$$h(\tilde{\theta}, \tilde{\varphi}, 0) = 1.0 + 0.1\, e^{-(\frac{\tilde{\theta}^2}{400} + \frac{(\tilde{\varphi}-80)^2}{25})},$$

and initial velocities are set to zero. Again, periodic boundary conditions are prescribed in the eastern and western boundaries. Figures 6 and 7 shows the evolution of the initial perturbation through the North pole. Observe that the proposed numerical treatment at the poles seems to perform well and no spurious wave are created.

5.4 Propagation of a wave initially confined between two meridians

In this test we simulate the evolution of a barotropic wave initially confined between two meridians over a uniform bathymetry. Here, the complete sphere is considered, that is the rectangular domain in the $\tilde{\theta}$-$\tilde{\varphi}$ plane is given by $[-180, 180] \times [-90, 90]$ with the spatial resolution $\Delta_{\tilde{\theta}} = \Delta_{\tilde{\varphi}} = 0.25°$. The depth is assumed to be constant $H(\tilde{\theta}, \tilde{\varphi}) = 1$m and the initial water thickness is given by

$$h(\tilde{\theta}, \tilde{\varphi}, 0) = 1.0 + 0.1\, e^{-\frac{\tilde{\theta}^2}{10}} + 0.1\, e^{-\frac{(|\tilde{\theta}|-180)^2}{10}}.$$

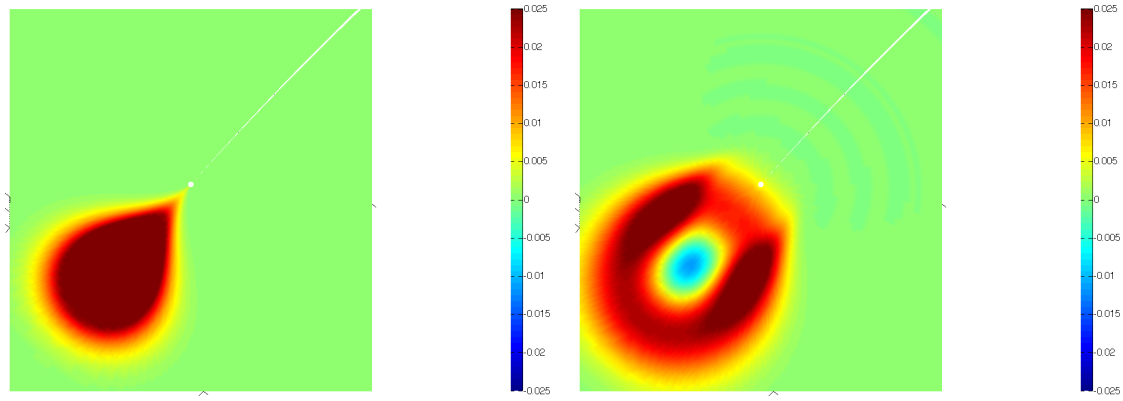

(a) Free surface at $t = 0$ minutes (b) Free surface at $t = 4$ minutes

Figure 6: Evolution of the free surface through the North pole.

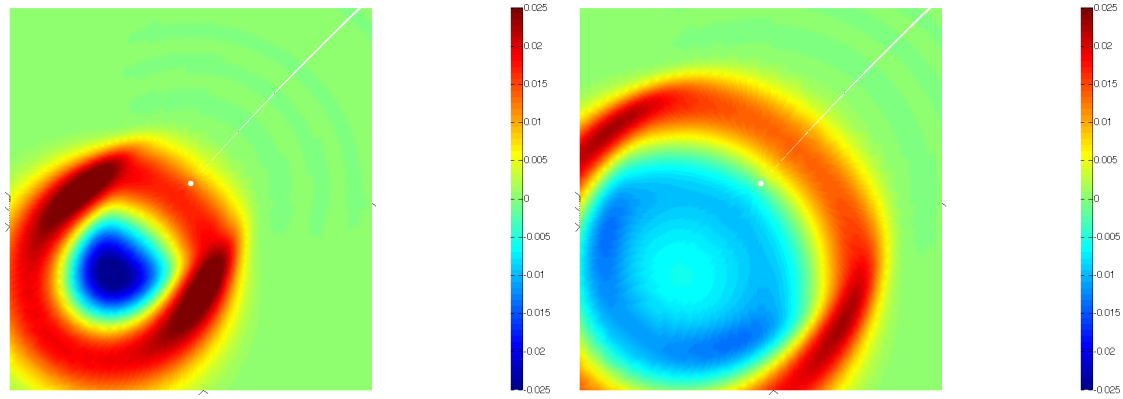

(a) Free surface at $t = 6$ minutes (b) Free surface at $t = 12$ minutes

Figure 7: Evolution of the free surface through the North pole.

The initial velocities are again set to zero. Here, we consider the same boundary conditions than in the previous test, and CFL is set again to 0.5. The evolution of the free surface is shown in Figures 8 and 9. In this case, the initial profile is split into two waves traveling eastward and westward respectively (see Figure 8(b)). After approximately 80 minutes both waves collapse around the eastern and western poles (see Figure 9(a)) generating two waves traveling in the opposite direction of the initial ones (see Figure 9(b)).

5.5 Propagation of a wave initially confined between two parallels

This test is similar to the previous one and the same domain, resolution, CFL parameter, radius, and boundary conditions are considered. Here, we simulate the evolution of a barotropic wave initially confined between two parallels over a uniform bathymetry. The initial water thickness is given by

$$h(\tilde{\theta}, \tilde{\varphi}, 0) = 1.0 + 0.1e^{-\frac{\tilde{\varphi}^2}{10}}$$

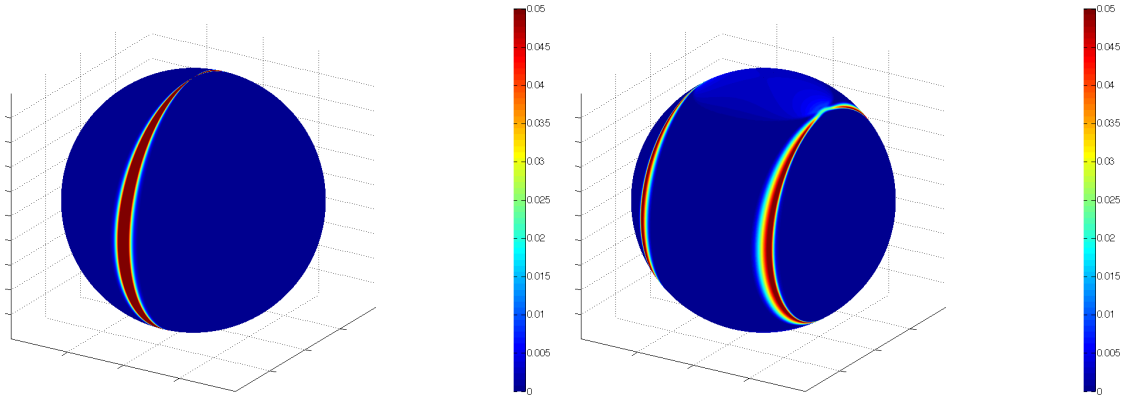

(a) Free surface at $t = 0$ minutes.

(b) Free surface at $t = 30$ minutes.

Figure 8: Wave confined between two meridians: free surface evolution.

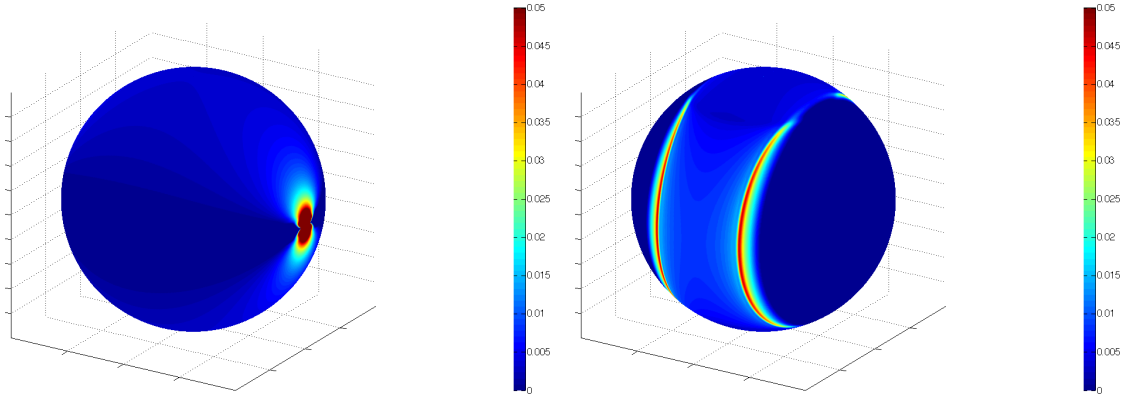

(a) Free surface at $t = 80$ minutes

(b) Free surface at $t = 135$ minutes

Figure 9: Wave confined between two meridians: free surface evolution.

and the initial velocities are again set to zero. The evolution of the free surface is shown in Figures 10 and 11. As in the previous numerical test, the initial profile splits into two waves traveling northward and southward respectively (see Figure 10(b)). After approximately 80 minutes both waves collapse around the north and south poles (see Figure 11(a)) generating two waves traveling in the opposite direction of the initial ones (see Figure 11(b)).

5.6 Order of convergence

The aim of this test is to check the empirical order of convergence of the numerical scheme. Here we consider four different uniform structured grids of the rectangular domain in the $\tilde{\theta}$-$\tilde{\varphi}$ plane given by $[-180, 180] \times [-88, 88]$ with $\Delta^l_{\tilde{\theta}} = \Delta^l_{\tilde{\varphi}} = 8°/2^l$, $l = 0, \cdots, 3$ of a sphere of radius $R = 10000$ m. The bathymetry and initial condition are given by:

$$H(\tilde{\theta}, \tilde{\varphi}) = 1.0 - 0.5\, e^{-\frac{\tilde{\theta}^2 + \tilde{\varphi}^2}{100}},$$

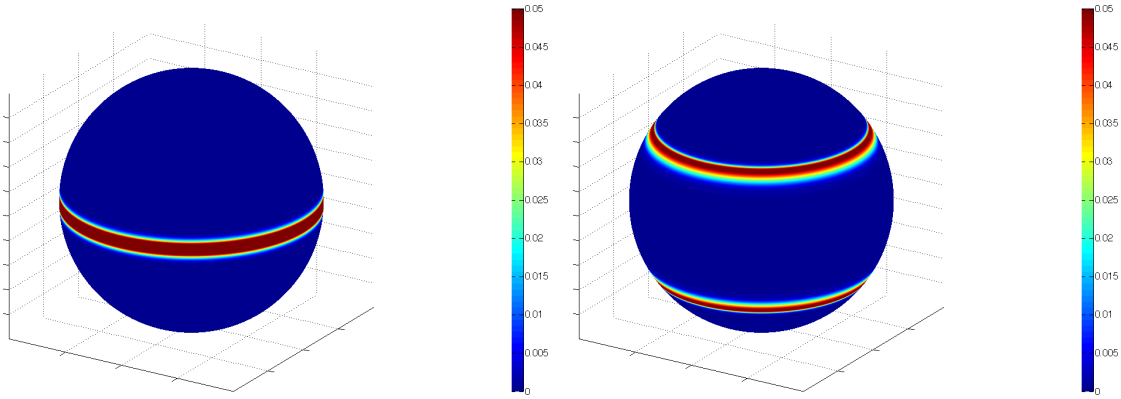

(a) Free surface at $t = 0$ minutes.

(b) Free surface at $t = 30$ minutes.

Figure 10: Wave confined between two parallels: free surface evolution.

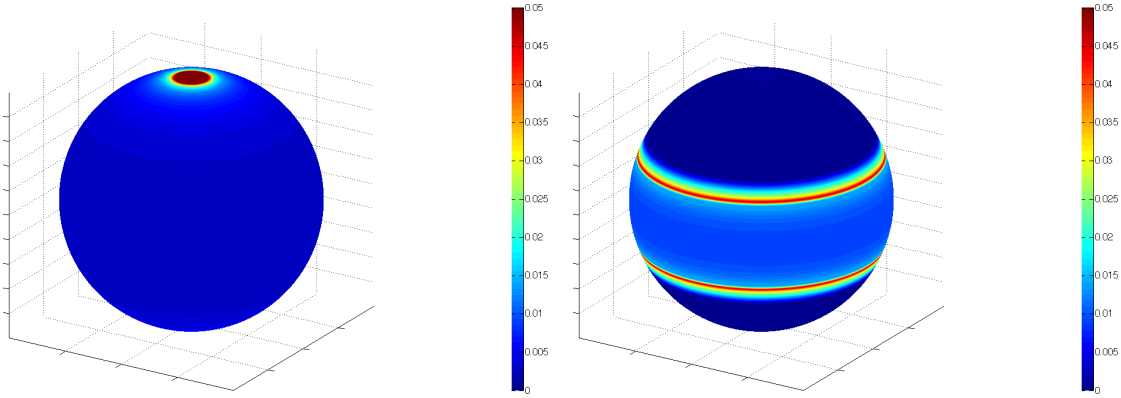

(a) Free surface at $t = 80$ minutes

(b) Free surface at $t = 135$ minutes

Figure 11: Wave confined between two parallels: free surface evolution.

$$h(\tilde{\theta}, \tilde{\varphi}, 0) = 1.0 - 0.5\, e^{-\frac{\tilde{\theta}^2+\tilde{\varphi}^2}{100}} + 0.1\, e^{-\frac{\tilde{\theta}^2+\tilde{\varphi}^2}{50}},$$

$$v_{\tilde{\theta}}(\tilde{\theta}, \tilde{\varphi}, 0) = -0.1\tilde{\varphi} e^{-\frac{\tilde{\theta}^2+\tilde{\varphi}^2}{50}}, \quad v_{\tilde{\varphi}}(\tilde{\theta}, \tilde{\varphi}, 0) = 0.1\tilde{\theta} e^{-\frac{\tilde{\theta}^2+\tilde{\varphi}^2}{50}}.$$

Periodic boundary conditions are prescribed in the eastern and western boundaries and open boundary conditions are set in the northern and southern boundaries. The system is integrated up to time $t = 600$ s. The CFL parameter is set to 0.5. A reference solution has been computed in a fine mesh with $\Delta_{\tilde{\theta}} = \Delta_{\tilde{\varphi}} = 0.125°$.

Table 2 shows the errors in L^1-norm and the order of convergence for the solution at $t = 600$ s. As expected, third order accuracy is achieved.

Figures 12 and 13 show the bathymetry, the water depth, and the velocities $v_{\tilde{\theta}}$ and $v_{\tilde{\varphi}}$, respectively for the grid with resolution $\Delta_{\tilde{\theta}} = \Delta_{\tilde{\varphi}} = 1°$.

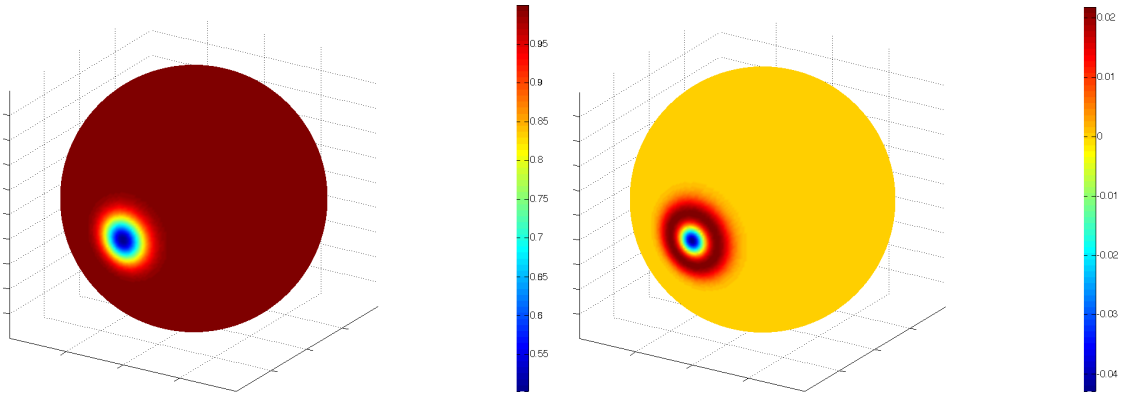

(a) Bathymetry. (b) Free surface at $t = 600$ s.

Figure 12: Bathymetry and Free surface at $t = 600$ s.

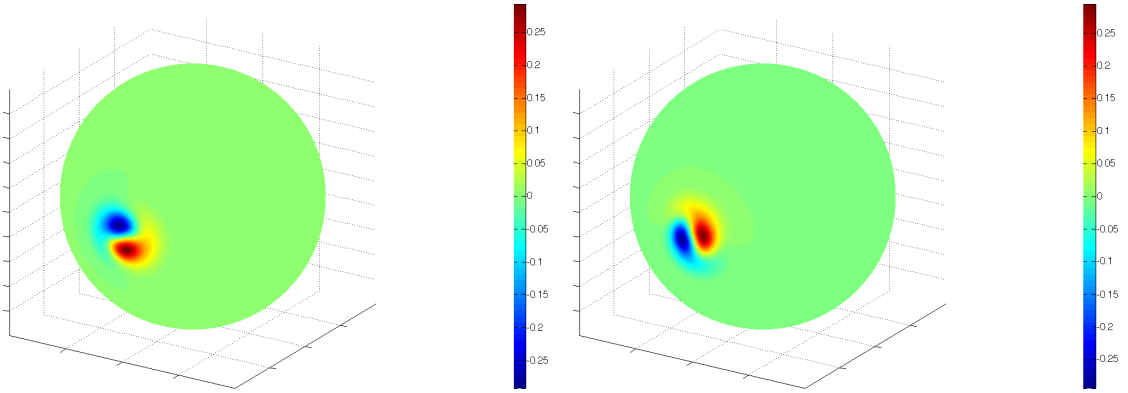

(a) v_θ at $t = 600$ s. (b) v_φ at $t = 600$ s.

Figure 13: v_θ and v_φ at $t = 600$ s.

5.7 Hypothetical tsunami in the eastern Mediterranean basin

In this test we simulate the evolution of a hypothetical tsunami in the eastern Mediterranean basis. A uniform cartesian grid of the rectangular domain in the $\tilde{\theta}$-$\tilde{\varphi}$ plane given by $[6.25, 36.25] \times [30.25, 45.65]$ with $\Delta_{\tilde{\theta}} = \Delta_{\tilde{\varphi}} = 30''$. The mean radius of the Earth is set to $R = 6371009.4$ m and the CFL parameter is set to 0.5. Open boundary conditions are prescribed at the four boundaries. The topo-bathymetry of the area has been interpolated from the ETOPO1 Global Relief Model (see [5]). Next, a hypothetical seafloor deformation generated by an earthquake of magnitude $M_s = 8$ has been computed using the Okada model (see [28]). This seafloor deformation is instantaneously transmitted to the water column to generate the initial tsunami profile (see Figure 14(a)). The initial velocity is set to zero. Concerning the numerical treatment of wet/dry fronts, here we follow the ideas described in [18], that have been adapted to the reconstruction operator defined in [17]. Figures 14 and 15 show the evolution of the tsunami wave propagating along the eastern Mediterranean Sea. Note that after approximately one hour, the waves generated near to the Greek coasts, arrive to the north of Africa and south of Italy (see Figures 14 and 15).

$\Delta \mathbf{x}$	Error h_σ	Order	Error Q_θ	Order	Error Q_φ	Order
$8°$	$3.09E-3$	-	$2.23E-3$	-	$1.08E-3$	-
$4°$	$4.18E-4$	2.89	$3.58E-4$	2.64	$2.78E-4$	1.94
$2°$	$5.54E-5$	2.92	$4.35E-5$	3.04	$3.23E-5$	3.12
$1°$	$6.61E-6$	3.07	$4.87E-6$	3.16	$3.79E-6$	3.09

Table 2: Error (L^1-norm) and order of convergence.

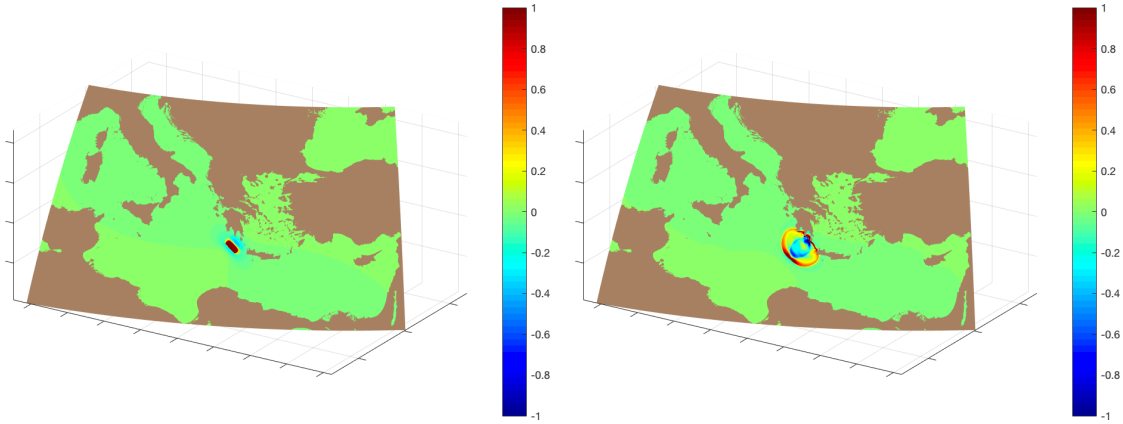

(a) Free surface at $t = 0$ minutes.

(b) Free surface at $t = 10$ minutes.

Figure 14: Evolution of a hypothetical tsunami at the eastern Mediterranean basin.

6 Conclusions

A high order finite volume well-balanced method for the SWEs in spherical coordinates have been presented. To do that, first the system has been rewritten in the form of a system of balance laws using a new set of unknowns. Then, a numerical scheme based on a first order path-conservative scheme and high order reconstruction operators is derived. Although the PDE system is formally similar to the SWEs in Cartesian coordinates, the new source term $G_\varphi(W)\partial_\varphi \sigma$ appears. Due to this and to the fact that, in the selected unknowns, the expression of water at rest solutions is more complex, the preservation of these stationary solutions is not as straightforward as in Cartesian coordinates case. Nevertheless, it has been proved that the numerical method is well-balanced if both the first-order path-conservative method is well-balanced for the standard 1d SWEs and the reconstruction operator is also well-balanced. A non-standard reconstruction procedure is proposed on the basis of a standard reconstruction operator that is well-balanced and high order accurate. A GPU parallel implementation has been performed in order to reduce the computational cost. Finally, some numerical tests to check the well-balancing and high order properties of the scheme, as well as its ability to simulate planetary waves or tsunami waves over realistic bathymetries have been presented. Future work will consist in adding the Coriolis force and non-hydrostatic effects that are relevant for the simulation of storm surge phenomena. Discontinuous Galerkin extensions of the method proposed here will be developed as well.

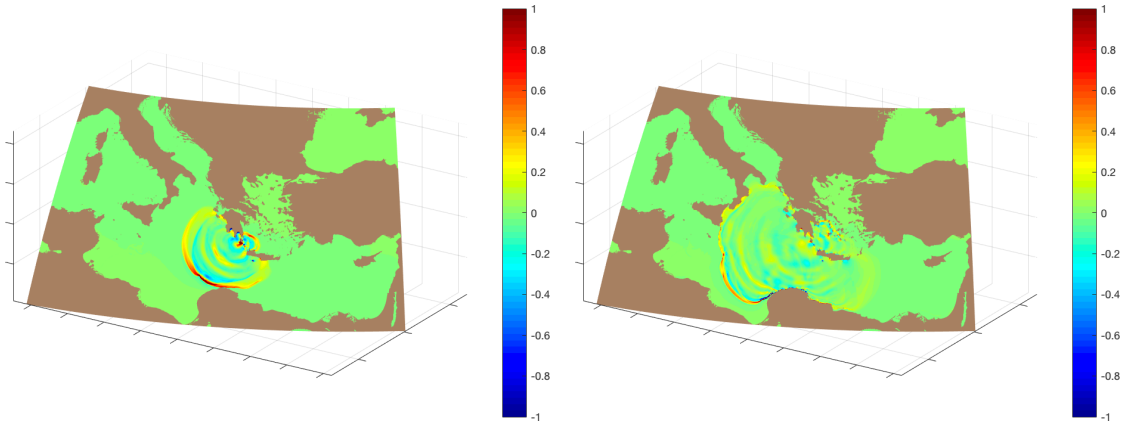

(a) Free surface at $t = 30$ minutes

(b) Free surface at $t = 60$ minutes

Figure 15: Evolution of a hypothetical tsunami at the eastern Mediterranean basin.

References

[1] E. Audusse, F. Bouchut, M. O. Bristeau, R. Klein, and B. Perthame. A fast and stable well-balanced scheme with hydrostatic reconstruction for shallow water flows. *SIAM Journal on Scientific Computing*, 25:2050–2065, 2004.

[2] A. Babeyko. *EasyWave: fast tsunami simulation tool for early warning.* Postdam University, 2012.

[3] A. Bermúdez and M. E. Vázquez. Upwind methods for hyperbolic conservation laws with source terms. *Computers & Fluids*, 23(8):1049–1071, November 1994.

[4] F. Bouchut. *Nonlinear stability of finite volume methods for hyperbolic conservation laws and well-balanced schemes for sources.* Frontiers in Mathematics. Birkhäuser Verlag, Basel, 2004.

[5] B. W. Eakins C. Amante. Etopo1 1 arc-minute global relief model: Procedures, data sources and analysis. Technical report, National Geophysical Data Center, NOAA, 2009.

[6] M. Castro, E. Fernández-Nieto, A. Ferreiro, J. García-Rodríguez, and C. Parés. High order extensions of Roe schemes for two-dimensional nonconservative hyperbolic systems. *Journal of Scientific Computing*, 39(1):67–114, 2008.

[7] M. Castro, J. M. Gallardo, and C. Parés. High order finite volume schemes based on reconstruction of states for solving hyperbolic systems with nonconservative products. Applications to shallow-water systems. *Mathematics of computation*, 75(255):1103–1134, 2006.

[8] M.J. Castro, T. Morales de Luna, and C. Parés. *Handbook of Numerical Methods for Hyperbolic Problems. Vol. 18 – Applied and Modern Issues: Well-Balanced Schemes and Path-Conservative Numerical Methods*, pages 131–175. Handbook of Numerical Analysis. North Holland, 2017. ISBN: 9780444639103

[9] M.J. Castro, J.M. Gallardo, J.A. López, and C. Parés. Well-balanced high order extensions of Godunov method for linear balance laws. *SIAM Journal on Numerical Analysis*, 46:1012–1039, 2008.

[10] M. J. Castro Díaz, E. D. Fernández, G. Narbona-Reina, and M. de la Asunción. A second order PVM flux limiter method. Application to magnetohydrodynamics and shallow stratified flows. *Journal of Computational Physics*, 262:172–193, April 2014.

[11] M. J. Castro Díaz and E. Fernández-Nieto. A class of computationally fast first order finite volume solvers: PVM methods. *SIAM Journal on Scientific Computing*, 34(4):2173–2196, January 2012.

[12] T. Chacón Rebollo, A. Domínguez Delgado, and E. D. Fernández Nieto. A family of stable numerical solvers for the shallow water equations with source terms. *Computer Methods in Applied Mechanics and Engineering*, 192(1-2):203–225, January 2003.

[13] I. Cravero and M. Semplice. On the accuracy of weno and cweno reconstructions of third order on nonuniform meshes. *Journal of Scientific Computing*, 67(3):1219–1246, 2016.

[14] M. de la Asunción, M. J. Castro, E. D. Fernndez-Nieto, J. M. Mantas, S. Ortega-Acosta, and J. M. González-Vida. Efficient gpu implementation of a two waves tvd-waf method for the two-dimensional one layer shallow water system on structured meshes. *Computers & Fluids*, 80:441 – 452, 2013. Selected contributions of the 23rd International Conference on Parallel Fluid Dynamics ParCFD2011.

[15] M. Dumbser, C. Enaux, and E. F. Toro. Finite volume schemes of very high order of accuracy for stiff hyperbolic balance laws. *Journal of Computational Physics*, 227(8):3971–4001, April 2008.

[16] M. Dumbser and C. D Munz. Building Blocks for Arbitrary High Order Discontinuous Galerkin Schemes. *Journal of Scientific Computing*, 27(1-3):215–230, December 2005.

[17] J. M. Gallardo, S. Ortega, M. de la Asunción, and J. M. Mantas. Two-dimensional compact third-order polynomial reconstructions. solving nonconservative hyperbolic systems using gpus. *Journal of Scientific Computing*, 48(1):141–163, 2011.

[18] J. M. Gallardo, C. Parés, and M. Castro. On a well-balanced high-order finite volume scheme for shallow water equations with topography and dry areas. *Journal of Computational Physics*, 227(1):574 – 601, 2007.

[19] S. Gottlieb and C-W. Shu. Total variation diminishing Runge-Kutta schemes. *Mathematics of Computation of the American Mathematical Society*, 67(221):73–85, 1998.

[20] A. Harten, B. Engquist, S. Osher, and S. R. Chakravarthy. Uniformly High Order Accurate Essentially Non-oscillatory Schemes, III. *Journal of Computational Physics*, 131(1):3–47, February 1997.

[21] A. Harten, P. D. Lax, and B. Van Leer. On upstream differencing and godunov-type schemes for hyperbolic conservation laws. *SIAM Review*, 25(1):35–61, 1983.

[22] R. J. LeVeque. Balancing source terms and flux gradients in high-resolution Godunov methods: the quasi-steady wave-propagation algorithm. *Journal of Computational Physics*, 146(1):346–365, 1998.

[23] M. Lukáčová-Medvid'ová, S. Noelle, and M. Kraft. Well-balanced finite volume evolution Galerkin methods for the shallow water equations. *Journal of Computational Physics*, 221(1):122–147, January 2007.

[24] J. M. Mantas, M. de la Asunción, and M. J. Castro. *An Introduction to GPU Computing for Numerical Simulation*, pages 219–251. Springer International Publishing, Cham, 2016.

[25] A. Marquina. Local Piecewise Hyperbolic Reconstruction of Numerical Fluxes for Nonlinear Scalar Conservation Laws. *SIAM Journal on Scientific Computing*, 15(4):892–915, July 1994.

[26] S. Noelle, N. Pankratz, G. Puppo, and J. R. Natvig. Well-balanced finite volume schemes of arbitrary order of accuracy for shallow water flows. *Journal of Computational Physics*, 213(2):474–499, 2006.

[27] S. Noelle, Y. Xing, and C.-W. Shu. High-order well-balanced finite volume WENO schemes for shallow water equation with moving water. *Journal of Computational Physics*, 226(1):29–58, 2007.

[28] Y. Okada. Surface deformation due to shear and tensile faults in a half space. *Bulletin of the Seismological Society of America,*, 75:1135 – 1154, 1985.

[29] C. Parés. Numerical methods for nonconservative hyperbolic systems: a theoretical framework. *SIAM Journal on Numerical Analysis*, 44(1):300–321 (electronic), 2006.

[30] C. Parés and M.J. Castro. On the well-balance property of Roe's method for nonconservative hyperbolic systems. Applications to shallow-water systems. *ESAIM: Mathematical Modelling and Numerical Analysis*, 38(5):821–852, 2004.

[31] J. Pedlosky. *Geophysical Fluid Dynamics.* Springer-Verlag, second edition edition, 1987.

[32] Y.S. Cho P.L.F. Liu, S.B. Woo. *Computer programs for tsunami propagation and inundation.* Technical report, Cornell University, 1998.

[33] G. Russo and A. Khe. High order well balanced schemes for systems of balance laws. In *Hyperbolic problems: theory, numerics and applications*, volume 67 of *Proc. Sympos. Appl. Math.*, pages 919–928. Amer. Math. Soc., Providence, RI, 2009.

[34] C.-W. Shu and S. Osher. Efficient implementation of essentially non-oscillatory shock-capturing schemes. *Journal of Computational Physics*, 77(2):439–471, August 1988.

[35] H. Tang, T. Tang, and K. Xu. A gas-kinetic scheme for shallow-water equations with source terms. *Zeitschrift für angewandte Mathematik und Physik ZAMP*, 55(3):365–382, May 2004.

[36] E. F. Toro. A Weighted Average Flux Method for Hyperbolic Conservation Laws. *Proceedings of the Royal Society of London A: Mathematical, Physical and Engineering Sciences*, 423(1865):401–418, June 1989.

[37] E. F. Toro and S. J. Billett. Centred TVD schemes for hyperbolic conservation laws. *IMA Journal of Numerical Analysis*, 20(1):47–79, January 2000.

[38] E. F. Toro, M. Spruce, and W. Speares. Restoration of the contact surface in the hll-riemann solver. *Shock Waves*, 4(1):25–34, 1994.

[39] E. F. Toro. *Shock-Capturing Methods for Free-Surface Shallow Flows.* Wiley and Sons Ltd, Chichester, 2001.

[40] T. Weiyan. *Shallow water hydrodynamics.* Elsevier Oceanography series,1992.

[41] Y. Xing. *Handbook of Numerical Methods for Hyperbolic Problems. Vol. 18 – Applied and Modern Issues: Numerical Methods for the Nonlinear Shallow Water Equations*. pages 361–384. Handbook of Numerical Analysis. North Holland, 2017. ISBN: 9780444639103

[42] Y. Xing and C.-W. Shu. High order well-balanced finite volume WENO schemes and discontinuous Galerkin methods for a class of hyperbolic systems with source terms. *Journal of Computational Physics*, 214(2):567–598, May 2006.